PCCP

Accepted Manuscript

ROYAL SOCIETY OF CHEMISTRY

www.rsc.org/pccp

Nucleation and growth kinetics of zirconium-oxo-alkoxy nanoparticles

Sana Labidi, Zixian Jia, Mounir Ben Amar, Khay Chhor and Andrei Kanaev[#]

Laboratoire des Sciences des Procédés et des Matériaux, CNRS, Université Paris 13, Sorbonne Paris Cité, 93430 Villetaneuse, France

[#] Corresponding author. E-mail: andrei.kanaev@lspm.cnrs.fr

Abstract

Nucleation and growth of zirconium-oxo-alkoxy (ZOA) nanoparticles was studied in the sol-gel process in n-propanol solution at the hydrolysis ratio H between 1.0 and 2.7 and zirconium-n-propoxyde precursor concentrations between 0.10 and 0.15 mol/l. The chemical transformations were conducted in quasi-perfect micromixing conditions (Damköhler number Da≤1) and the nanoparticles size evolution was monitored in situ with the light scattering method. The size of primary nanoparticles (nuclei) $2R_0$=3.6 nm was found to be almost independent on the preparation conditions. A remarkable similarity with the titanium-oxo-alkoxy (TOA) nanoparticles was observed. In particularly, both systems show the induction stage of the sol-gel growth for hydrolysis ratio H>2.0 and stable oxometallate units for H≤2.0. However in contrast to TOA, no stable hierarchical ZOA units (clusters) with $R_0 \geq R \geq 1.0$ nm were observed, which makes this system less stable against aggregation leading to polydispersed nanoparticles.

Keywords: zirconium-oxo-alkoxy nanoparticles, sol-gel process, growth kinetics.

1. Introduction

The basic sol-gel chemistry of metal alkoxides has been extensively studied over past decades and is rather deeply understood [1-3]. However, the general picture of the nucleation-growth of solids still requires improvements, which would permit a control the material fabrication process [4-5]. In particular, recent studies of the structure and reactivity of molecular precursors have shown the hypothesis of kinetically controlled hydrolysis-polycondensation process to be inconsistent. In contrast to the unconsciously accepted, the hydrolysis does not proceed for homometallic titanium or zirconium alkoxides via hydroxide intermediates but results directly in well-defined oligonuclear oxo-alkoxide species through one-step hydrolysis-condensation transformation associated with profound restructuring of the oxometallate species as the reactions progress [6-7]. Different soft chemistry processes occurring in gas, liquid and solid phases share common features of nanomaterial formation from precursor to solid, which require further investigation [3].

Several thermodynamically stable structural units (clusters) have been discovered among titanium-oxo-alkoxy species [8]. The size of the identified clusters is generally small (≤1 nm) and limited by the capacity of calculation methods that validate their existence. In the same time, larger well-defined nanometric-size species with hundreds and even thousands of constituting metal atoms are also expected [6]. In confirmation of this hypothesis, our group has recently shown a formation of stable titanium-oxo-alkoxy (TOA) particles of 2.0, 3.2 and 5.2 nm size in 2-propanol solutions triggered by hydrolysis-condensation reactions between titanium-tetra-isopropoxide (TTIP) and water molecules [9]. The “classical” induction stage of the sol-gel growth involves 5.2 nm particles, which were called nuclei. These TOA nanoparticles remain however the only example reported until now and generalization of the nucleation mechanism discovered in titania to other systems remains an important issue in the domain of sol-gel science.

Zirconia oxo-alkoxy (ZOA) sol-gel synthesis involving reactive metal alkoxide precursors and alcohol solvents is rather similar to that of TOA. Despite little is known about molecular ZOA compounds, key role of the tetrameric zirconyl units in the formation of hydrous amorphous ZrO_2 precipitates has been suggested [10]. $Zr_3O(O^tBu)_9(OH)$ cluster with the molecular geometry practically identical to $Ti_3O(O^iPr)_{10}$ has been reported [11]. More recently, $Zr_4O(O^nPr)_{14}(^nPrOH)_2$ [12] and $Zr_3O(O^tBu)_{10}$ molecular clusters have been evidenced and thoroughly investigated [13]. The hierarchically bigger ZOA nanoparticles formed of these nanoclusters can appear as the smallest constituent of zirconia solids. Several groups have previously reported on the smallest structural units of zirconia solids obtained after the sol-gel synthesis [14-20]. However, most of these studies concerned the crystalline domains between 5 and 100 nm observed after the thermal treatment, which does not allow directly extrapolating to the basic ZOA units. The zirconia nuclei in amorphous precipitates were reported to be in the range of 1.3-1.8 nm depending on pH, associated in 2D fractals and conserved their local structure in course of crystallization [21-24]. In the same time, the nucleation-growth process kinetics of zirconia solids in the sol-gel synthesis has never been documented so far.

The structure of many of these oxo- or hydroxo-species is expected to be thermodynamically stable and independent on the way of their preparation. Moreover, these basic metal oxo-alkoxy units define in many respects useful properties of the final materials, including coatings and bulk solids [25-26]. Knowledge of these basic units and their reactivity control is an important issue, which solution opens many interesting applications in nanotechnologies: biomedicine [27], photonics [28], protective coatings [29], catalysis [30] and solar cells [31].

A high intrinsic reactivity of the basic metal oxo-alkoxy clusters and nanoparticles makes their preparation in macroscopic quantities challenging and a standard sol-gel synthesis

generally leads to strongly polydispersed colloids. Moreover, using stabilisation agents is undesirable because of the possible modification of their size, shape and related electronic properties. This strong polydispersity prohibits identification of units in correlation with their size-specific properties. A solution to preparation of macroscopic quantities of size-selective clusters and nanoparticles consists in the rapid micromixing of the reaction components [32]. When the micromixing time becomes shorter compared to the characteristic time of the reactions, the chemical system attains the narrowest polydispersity. With this objective, we have developed a sol-gel reactor with micromixing time below 10 ms [33-34], which is shorter than primary hydrolysis-condensation reaction leading to nucleation [35]. The hierarchical mechanism of sol-gel growth and decrease of the unit's reactivity with size permit fabrication of macroscopic quantities of size-selective TOA nanoparticles for integration in functional materials [26, 36-37].

In the present communication we report on the nucleation-growth process kinetics of ZOA nanoparticles realised in quasi-perfect micromixing conditions (Damköhler number $Da \leq 1$) of alcoholic solutions containing zirconium alkoxides precursors and water. Size of the growing clusters and nanoparticles was monitored in situ by the dynamical light scattering method.

2. Experiment

The sol-gel process involving ZOA species was conducted in the sol-gel reactor with rapid micromixing described in Refs [33-34]. The main part of this reactor is the T-mixer of Hartridge and Roughton type with an eccentric reagents injection, which permits the turbulent flow of fluids at Reynolds numbers ($Re=4Q\rho/\pi\eta d$, where Q, ρ, and η are the fluid flow rate, density and dynamic viscosity) above 500. Two thermostatic stock solutions (maintained at 20.0 °C with a thermo-cryostat Haake, DC10K15), containing alcoholic solutions of ZOA

precursors (A) and water (B), were injected into the mixer at flow rates above ~10 m/s by applying an external gas pressure (N_2), which maintains Re≈6000 along the mixer inlet and main outlet channels. In these experimental conditions, the micromixing of the reacting fluids is completed on the timescale of several milliseconds [34], which is expected to be shorter than characteristic hydrolysis-condensation reactions leading to the formation of subnuclei clusters and nucleation of nanoparticles. The optimal operating regime of the sol-gel reactor corresponds to the Damköhler number Da≤1 that permits the smallest polydispersity of the produced units.

In present experiments we examined the reaction media containing precursors zirconium n-butoxide (ZNB) (80 wt.% supplied by Sigma-Aldrich) and zirconium n-propoxide (ZNP) (70 wt.% supplied by Interchim), solvents n-propanol (≥99.5 % supplied by Sigma-Aldrich), 2-propanol (≥99.5 % supplied by Acros), n-butanol (≥99.4 % supplied by Sigma-Aldrich), and ethanol (≥99.8 % supplied by Fulka) and distillated, demineralized and twice-filtered water (syringe filter 0.1 µm porosity PALL®Acrodisc). The precursors concentration and hydrolysis ratio H ($H=C_{H2O}/C_{Zr}$) were varied in the range 0.1-0.15 mol/l and 1.0-2.7, respectively. We notice that the residual water content in the alcohols <0.2 % corresponds to the hydrolysis ratio <0.07 in standard experimental conditions (0.15 mol/l precursor in 100 ml reactor volume). To avoid any alcohol contamination with atmospheric humidity, the bottle with alcohol was kept hermetically closed in the LABstar high-quality glove box workstation MBraun (purified from O_2 gas and H_2O vapour; H_2O vapour pressure <0.5 ppm) no longer than four weeks after the first opening.

The sol-gel kinetics has a high sensitivity to water content in the reactive solution. Therefore to avoid an uncertainty of the hydrolysis ratio, possible contamination of the reactor volume by water vapour was verified. The correct operation conditions have been checked by measuring the induction kinetics. More often, a solution of 0.15 mol/l titanium tetra-iso-

propoxide at H=2.5 was used as reference: the reaction conditions were judged satisfactory if the induction time fits 50±5 min. Consequently, the uncertainty of the hydrolysis ratio was estimated H±0.05. The preparation and feeding of the syringes with two stock solutions A and B were also performed in the glove box. The feeding of the respective reactor reservoirs from syringes was performed by keeping the reactor volume under the dry nitrogen gas pressure ~0.5 bar above the atmospheric pressure in order to avoid any contamination of the reactive solutions by atmospheric humidity. We notice that the ZOA precursor and water concentrations in the stock solutions, each of 50 ml volume, were twice higher than those in the reactive solution of 100 ml volume after the mixing.

The particle size (2R, nm) and scattered light intensity (I, Hz) measurements in the reactor were performed by DLS (dynamic light scattering) and SLS (static light scattering) methods using a monomode optical fiber probe, 40 mW / 640 nm single-frequency laser Cube 640-40 Circular (Coherent) and 48 bits 288 channels photon correlator Photocor-PC2 (PhotoCor Instruments). The observation volume defined by a mutual positioning of two monomode optical fibres is small enough (~10^{-6} cm^3) to avoid multiple scattering events even in high-concentration colloids. The measurements (I,R) were carried out in the automatic sampling mode with the data accumulation period of 60 s, which permits easy rejection of non-desirable events due to rare dust particles producing strong light scattering spikes and accumulation a good signal-to-noise ratio even from small (R~1 nm) particles. The stability of the reactive solution was controlled to avoid a decrease of the temporal resolution of the growth kinetics, and the signal accumulation was only applied on a time-scale of the mean cluster size stability. The experimental series were limited by 48 hours duration. Beyond this time we were not capable to guarantee non-contamination of the reaction solutions by an atmospheric humidity.

The particle radius is derived from Einstein-Stokes formula $R = k_B T q^2 \tau / 3\pi\eta$ (k_B, T, $q = 4\pi n / \lambda \cdot \sin(\theta/2)$, η and n are correspondingly Boltzmann constant, temperature, scattering vector, dynamic viscosity and refraction index of sample, and the decay time constant τ was experimentally obtained from the fit of autocorrelation curves (ACF)), as that of an equivalent spherical particle with the same diffusion coefficient. The practice shape can be however non-spherical, and its shape can be estimated from kinetics measurements [38]. The fractal dimension D_f of the growing structures was obtained from simultaneous measurements of the scattered light intensity I(t) and mean hydrodynamic radius R(t) of nanoparticles according to the expression $D_f = \frac{d(\ln(I))}{d(\ln(R))}$. Its validity is explained by the Rayleigh domain of the particle size ($R<<\lambda$) and conservation of the total mass of nanoparticles during the induction stage of sol-gel process: $I \propto Nm^2 = Mm \propto R^{Df}$ (where N, M and m are total number and mass and individual mass of nanoparticles).

3. Results and Discussion

3.1. Polydispersity of ZOA sols

The classical LaMer nucleation model [39] appears to be not appropriate for the description of induction kinetics of transition metal oxides. The condensed oxo-alkoxy species undergo the hierarchical growth [40]. We call “nucleus” the largest stable nano-unit that aggregate at the induction stage; these units keep their identity and can be distinguished in the precipitated powder. In contrast (as we have earlier shown on example of titania [9]), the nucleus is produced by condensation of small clusters associated with their restructuring.

The nucleation of ZOA species is extremely fast and proceeds on the millisecond timescale, similar to TOA. This was confirmed by the light scattering measurements, which evidence the appearance of nanoparticles immediately after the reacting fluids injection in the

T-mixer. This nucleation stage is followed by a relatively long period of the particles aggregation called induction period, after which the solution loses stability and ZOA species precipitate.

Despite of a seemingly simple and repetitive reaction sequence of the sol-gel synthesis, the nucleated units depend quite sensibly on the precursor and solvent natures. The ACFs of several sol-gel solutions measured after the reactive fluids mixing are shown in Figure 1 (a-d). The ZNB precursor reacting with water in n-butanol and 2-propanol solvents shows the presence of relatively large particles of size between 2R=100 and 500 nm and essentially multimodal particle size distribution. Although the large particles appear in ZNB/ H_2O/ethanol solutions, a small fraction of much smaller nanoparticles with 2R~4 nm was also observed. In contrast, the large particles were not observed after the mixing of ZNP/H_2O/n-propanol solutions, where only small nanoparticles appear. Based on these observations, a conclusion can be drawn about the ZOA nucleation process. The basic 4-nm ZOA nuclei are stable and conserved in different solvent environments. These smallest nanoparticles constitute bigger ones and the possibility of their direct observation is related to a competition between the hydrolysis-condensation and transalcoholysis reactions. In the above example, the transalcoholysis consists in a partial replacement of butoxy groups of ZNB precursor by propoxy and ethoxy groups of the solvents. As a result, hydrolysis-condensation rates of the successively reacting precursor groups vary, which leads to an inhomogeneity of the reaction kinetics and polydispersity of the produced ZOA species.

A possible alternative explanation of the observed variation of the particles polydispersity could be a formation of zirconyl groups Zr=O depending on the precursor nature and solvent environment. The double bond character has been previously attributed to the stretching vibration of zirconia in the range of 830-960 cm^{-1} [41], which however was disapproved in

later studies [42]. Our FTIR measurements of dried precipitated sols after the synthesis have evidenced no significant difference; by consequence, we reject this hypothesis.

The nucleation control and formation of monodispersed ZOA nuclei require the chemical process to be slower compared to physical micromixing (Da≤1). The latter rate is fixed in our experimental conditions by the fluids injection with Re=6000. Probably, the hydrolysis-condensation reactions involving ZNB precursor run more rapidly (compared to ZNP precursor), since they result in much larger particles. Consequently, poor micromixing can explain the stronger polydispersity of the prepared sols in Figure 1 (a-b) that screens the smallest nuclei observation. Due to the reversibility of transalcoholysis, a partial exchange of butoxy groups of the ZNB precursor by ethoxy groups reduces the reactivity and the smallest nuclei become observable. The best nuclei selectivity was observed in parent alcohol solutions of ZNP. Since a monodispersed particles population was achieved in these conditions, the ZNP/H_2O/n-propanol solutions were further considered for the analysis of ZOA species and their growth kinetics.

3.2. Sol-gel growth kinetics

Because of the high micromixing quality of the sol-gel solution, we realized homogeneous reaction conditions permitted a narrowest polydispersity of nucleated species and careful inspection of the process kinetics. Below we consider the nucleation-growth process of ZOA nanoparticles. Two principal kinetics domains with H≤2.0 and H>2.0 can be distinguished.

Domain H≤2.0

The measured ACF curves of ZOA nanoparticles in ZNP/n-propanol solution at low hydrolysis ratios H<2.0 are shown in Figure 2. They are characterized by a single exponential decay with time constant corresponding to particles with the radius R=1.8 nm. No deviation from the single exponential decay was observed, which evidence their negligible polydispersity. Moreover, these curves do not change their temporal shape during the

measurements time of more than 24 hours, which indicates significant colloid stability in the experimental conditions. On the other hand, these units appear quasi-instantaneously after the injection of reactive fluids on the millisecond timescale, which is characteristic of high reactivity of these molecular species. Because of the above features, we assign the observed nanoparticles to nuclei.

Domain H>2.0

At higher hydrolysis ratios, the common acceleration kinetics characteristic of sol-gel induction stage has been observed. The temporal variations of the scattered light intensity by the nanoparticles and of their size are shown in Figure 3. The nanoparticles appear immediately after the reactive fluids injection and their hydrodynamic radius increases with time. At the end of the induction period ($t=t_{ind}$) the particle size abruptly increases. This corresponds to the particles precipitation and appearance of turbidity in the initially transparent solution, which explains the strong increase of the scattered light intensity. The induction time was measured at the point of the scattered light intensity increase by a factor of 5 over the mean level due to the non-aggregated nanoparticles. According to the general picture of sol-gel process, the sol particles slowly aggregate into chains of low fractality. The fractal dimension of the growing ZOA nanoparticles during the induction stage is close to 1, which indicates nuclei association in quasi-linear chains. Indeed, our measurements show $D_f=1.35\pm0.2$ for H=2.3 and $D_f=1.05\pm0.4$ for H=2.1. Resent theoretical calculations of Sathiyanarayanan et al. [43] have shown that the free-energy barrier for aggregation from the mesocrystal state is smallest on the smallest facets, which perpetuates anisotropic growth. This may explain the observed quasi-linear associates of zirconia nuclei.

It is expected that the induction rate ($r_{ind}=1/t_{ind}$ [38]) increases with an increase of both reagents ZNP and H_2O concentrations. Indeed, Figure 3 shows that the induction period

shortens with an increase of H. The behaviour of the induction time with variation of the zirconium concentration shows the similar tendency (Figure 4).

3.3. Nucleation-growth mechanism

The nature of the induction stage of sol-gel synthesis has been previously discussed in the scientific literature. It appears to be inconsistent with the classical LaMer model of the hydrolysed monomers accumulation and nucleation (at the end of this stage) when their concentration increases above the critical one. In particularly, the hydrolysis and condensation processes can not be considered separately and proceed simultaneously resulting in the condensed species of an increased complexity [6-7]. The condensed species appear on the millisecond timescale during the reactive fluids contact. The largest stable nano-unit that undergoes an aggregative growth at the late stage called "induction stage" is called nucleus: it and can be distinguished in the precipitate. The duration of the induction stage critically depends on the water excess (that is on H-h*, in terms of hydrolysis ratio $H=C_{water}/C_{Ti}$) over that needed for the nuclei formation (h*). h* can be therefore assigned to the condensation ratio of nucleus, which defines its elemental composition. Consequently, the knowledge of h* is crucial for the understanding of the nucleus structure and that of the final solids. At the end of the induction stage, the nuclei aggregate forming bigger micronic-size particles that precipitate. The induction time characterises the build-up of the infinite fractal [33]. One can also address a recent review of mechanisms and kinetics of the aggregative growth of nanocrystals [44].

Tables 1 and 2 summarise the initial nanoparticles (nuclei) radius R_0 at the beginning of the induction period and the induction time (t_{ind}) in ZNP/H_2O/n-propanol solutions of different composition related to H and C_{Zr} components. The process intensifies with an increase of both H and C_{Zr} while the initial nuclei size remains almost stable. This behaviour is similar to that earlier established in case of the sol-gel growth of TOA nanoparticles [9].

Below we apply the earlier proposed description of the TOA nanoparticles growth [33, 38] to ZOA nanoparticles.

The basic feature of the earlier proposed model consists in an equivalence of the sol-gel process description in terms of induction rates and aggregation kinetics, which can be expressed as

$$r_{ind} = t_{ind}^{-1} \propto dI / dt \tag{1}$$

with the intensity scattered by the ensemble of sol nanoparticles

$$I \propto \mu_2(t) = \int_{m^*}^{\infty} m^2 F(m,t) dm \tag{2}$$

where μ_2 is the second momentum of the particle mass (m) distribution F(m,t). We notice that the normalised presentation of the kinetics permits an expression of the induction rates in units s^{-1}.

We have checked this equivalence hypothesis in case of the ZOA nanoparticles growth by plotting the induction rates defined by both presentations in (1). We notice that the use of particle size instead of intensity is allowed because of the low fractal dimension of aggregates $D_f = \ln(I)/\ln(R) \approx 1$, which provides dI/dt $\propto$ dR/dt. The result in Figure 5 shows that the equivalence holds for the induction stage of ZOA sols. We therefore assume that the basic mechanism of the particles agglomeration proposed by Rivallin et al. [33] is common and can be applied to the ZOA sol-gel growth.

Figure 6 summarises the obtained results regarding the ZOA nucleus size and growth rate at different hydrolysis ratios. It evidences the change of the reaction kinetics at $H=h_1=2.0$, which separates two domains of the colloid stability and induction growth. Moreover within the experimental error bar, the initial particle radius is conserved in the broad range of $1 \leq H \leq 2.5$: $R_0=1.8$ nm, which is characteristic of a stable nucleus.

In order to confirm the nucleus size, we have performed the TEM analysis of the colloidal particles appearing at the induction stage with H>2.0. The image presented in Figure 7 evidences quasi-identical spherical ZOA nanoparticles of size 2R=3.6 nm, which perfectly fits that of the nucleus measured in the sol-gel solutions. Consequently, this unit appears in the stability domain of the sol-gel process (H<2.0), which permits homogeneous nucleation and prohibits nanoparticles growth. This unit also appears at early stage of the sol-gel induction stage (H>2.0) and serves to be the building block of zirconia solids issued of the sol-gel process.

The hydrolysis of the i-th OR group of metal ion is generally considered as reversible. On the other hand, the formation of sols by surface oxolation reactions is irreversible. This irreversibility may include a critical step. In agreement with TOA species [38], we assume that the ZOA condensation by oxylation reaction of the k-th bond is irreversible, whereas the reactions with $j < k$ are at equilibrium ($1 \le i, j \le n$, n is the number of hydrolysable bonds per zirconium atom):

$$...Zr(OR)_{n-i+1}(OH)_{i-1} + H_2O \leftrightarrow ...Zr(OR)_{n-i}(OH)_i + ROH$$

$$...Zr(OR)_{n-i}O_{j-1}(OH)_{i-j+1} + OH... \xleftrightarrow{j<k} ...Zr(OR)_{n-i}O_j(OH)_{i-j} + H_2O$$

$$...Zr(OR)_{n-i}O_{j-1}(OH)_{i-j+1} + OH... \xrightarrow{j\ge k} ...Zr(OR)_{n-i}O_j(OH)_{i-j} + H_2O$$

This reaction mechanism, earlier proposed for the sol-gel growth of TOA nanoparticles [33, 38], can explain the induction kinetics that critically depend on the reagents concentrations:

$$r_{ind} = kC_{Zr}^{a}(C_{H_2O} - C_{H_2O}^{*})^{b} = kC_{Zr}^{a+b}(H - h^{*})^{b} \quad (3)$$

where k is the reaction constant and h^* is the critical hydrolysis ratio accounted for the nuclei formation, above which the aggregation growth of nuclei becomes possible [45]. The coefficients *a* and *b* in (3) describe the reaction order related to zirconium precursor and water molecules, which can be different from 1.

In order to experimentally evaluate the reaction orders *a* and *b* of ZOA nanoparticles, we have plotted r_{ind} versus zirconia concentration C_{Zr} and hydrolysis ratio H in logarithmic frames respectively in Figures 8 and 9. The linear fit of the data in Figure 8 is straightforward and results in the parameters sum $a+b=6.3\pm0.2$. The situation with H series is more complicated, since another unknown parameter h^* exists, which represents the critical water content necessary for the nucleus composition; the higher hydrolysis ratio $H>h^*$ enables the aggregative nuclei growth. In this respect, this value corresponds to the condensation ratio (number of bridged oxygens per zirconium atom), which characterizes the chemical composition of ZOA nucleus.

No reliable experimental information concerning the critical hydrolysis ratio of ZOA is available in literature. However, two limit values of 1.5 and 2.0 could be proposed. The first value (1.5) is characteristic of TOA system. Indeed, Soloviev et al. [45] has proposed this critical hydrolysis ration for TOA species, which later has been ascribed to the appearance of non-consumed hydroxyls on stable sub-nucleus TOA clusters with 2R=3.6 nm size [9]. The second value (2.0) corresponds to the hydrolysis ratio separating two distinct domains of the sol-gel kinetics (similar in both TOA and ZOA systems), above which the induction growth takes place. The fit of experimental data with $h^*=1.5$ and 2.0 shown in Figure 9 resulting in the reaction order $b=6.6$ and 2.4.

Based of the experimental series $r_{ind} = f_1(C_{Zr})$ and $r_{ind} = f_2(H - h^*)$, two possible sets of the reaction orders are listed in Table 3. One can clearly disapprove one set of these values obtained with $h^*=1.5$, since the derived reaction order *a* related to the zirconium precursor is negative. On the other hand, the set of model parameters $h^*=2.0$, $b=2.4$ and $a=3.9$ cannot be explained in framework of the previously proposed model [33, 38] since the zirconium reaction order (*a*) is higher than 1. We therefore also calculated another set of kinetic

parameters corresponding to *a*=1: h*≈1.7 and *b*=5, which conveys the growth model proposed for TOA species.

3.4. Comparison with other oxides

Because of a high reactivity of metal-oxo-alkoxy species [35] and kinetically non-separated hydrolysis-polycondensation stages, which results in a strong sensibility of the cluster morphology to reaction conditions [3, 6-7], there is a lack of reliable experimental data on sol-gel nucleation-growth kinetics. Moreover, most of material studies deal with strongly polydispersed samples that screen details of the nucleation-growth process.

Our experiments showed that it is more difficult to achieve small polydispersity of ZOA than TOA colloids. This can be explained by their higher reactivity. In fact, the smallest polydispersity in the precipitation process is expected in the regime of low Damköhler numbers $Da=r_{ind}/r_{mix}\leq 1$, where r_{mix} is the rate of physical mixing. The micromixing of our solutions is realised through the specific turbulent energy dissipated in the T-mixer, resulting in interpenetrated fluid eddies, which characteristic size can be described by the Kolmogorov length:

$$L_k = (\nu^3 / \varepsilon)^{1/4} \quad (4)$$

where ν is kinematic viscosity and ε is specific power input, which can be expressed as $\varepsilon = \Delta p Q / \rho V$ with Δp, Q, ρ and V being pressure drop, flow rate, mass density of solution and mixer volume). The time required for the reactive solution homogenizing depends on the turbulence time (eddies formation) and diffusion time (eddies dissipation). The injected solutions pass the turbulence zone of the sol-gel reactor in regime with Re=6000 during t_{turb}~1 ms [34], while the diffusion time is longer. In our experimental conditions, eddies scale down to $L_k\approx 5$ μm in size and dissipate on the timescale of $t_{diff} = L_k^2 / D \approx 10$ ms (D~10^{-9} m^2/s molecular diffusion coefficient). As a result, the Brownian dissipation of fluid eddies is longer

and limits the micromixing process. Consequently, shortening of the micromixing time requires braking of liquids into even smaller eddies, which required much higher ε according to Equation (4). We conclude that realization of the homogeneous reaction conditions and consequently small polydispersity of ZOA colloids is more problematic compared to that of TOA.

Our results indicate common features of TOA and ZOA sol-gel systems realized with the rapid micromixing at the millisecond timescale:

- formation of sub-nucleus clusters and stable colloids at hydrolysis ratio H<2;
- formation of nuclei at H=2.0;
- induction growth of sol nanoparticles at H>2;
- association of nanoparticles in quasi-linear chains at the induction stage;
- high reaction order (>1) of hydrolysis-condensation of metal-oxo-alkoxy species;

At the same time, a difference between TOA and ZOA systems exists related to the sub-nuclei clusters stability. In fact, TOA species form stable clusters of size 2.0 and 3.2 nm, while ZOA species demonstrates no such intermediate-size clusters and the nuclei show up already at a very small H~1. The previously evidenced stable molecular clusters Zr_3 and Zr_4 may be the only candidates for the intermediate molecular clusters in respectively Bu and ^{n}Pr solvents [11-13]. Apparently, these smallest molecular clusters (SMC) form nucleus in multiple reactive collisions accompanied by their profound structural reorganization. A successful collision producing the nucleus (case of ZOA) involves a considerably larger number n of SMCs compared to that m producing another stable intermediate cluster (case of TOA): n>>m. Consequently, the SMCs concentration decreases more slowly in the first case: $C \propto 1/\sqrt[n-1]{t}$ (of n-th order reaction). As a result, larger concentrations of the residual highly reactive species may remain in the ZOA solution after nucleation, which make the colloid less stable against aggregation.

We notice that the dependence $r_{ind} = f_2(H)$ in Figure 6 may include sub-nucleus ZOA clusters similar to that evidenced in TOA solutions. The weak size variation of these hypothetic clusters (by ΔR~0.2 nm) could take place in the range of H~1.25 and 1.7. Moreover, the above fit of experimental data with reaction orders *a*=1 and *b*=5 yields the critical h*≈1.7, which may correspond to the stable nucleus formation (Figure 6). The error bars of the present experiments were relatively large to permit reliable verification of this supposition. The accumulation of a considerably larger number of ACF curves (in order to improve signal-to-noise ratio) will clarify this issue. Whether larger stable sub-nucleus ZOA clusters exist or not remain an open question, which can be clarified in future theoretical quantum chemistry calculations.

The most adequate description of the reaction kinetics requires further analysis of Equation (3). Both ZOA and TOA systems show critical hydrolysis ratio $h^* \leq 2.0$ and total reaction order *a*+*b*≈6. Assuming that the reaction order related to zirconium precursor is *a*=1, that related to water consumption becomes *b*=5 in agreements with the model by Rivallin et al. [33, 38]. On the other hand, one could fix $h^*=2.0$ in Figure 6 as corresponding to the infinite time of the sol-gel solution stability, which in turn would increase the reaction order of reactions involving both zirconium and water (see Tables 1 and 3). Unfortunately, longer lasted experiments than 24-48 hours were no sense to perform because of the non-negligible contamination of the reaction solutions by atmospheric humidity. Moreover, slower alcoxylation reactions (not considered in the model) become dominant at longer times, which make the conclusions uncertain. Although the fit of the experimental data with $h^*=2.0$ provides the smallest standard deviation value (χ^2), we need reliable complementary data to approve (or disapprove) this value.

4. Conclusion

We studied the nucleation and growth of zirconium-oxo-alkoxy (ZOA) nanoparticles in n-propanol solutions at the hydrolysis ratio H between 1.0 and 2.7 and zirconium-n-propoxyde precursor concentration between 0.10 and 0.15 mol/l. The nanoparticles were nucleated in quasi-perfect micromixing conditions (Damköhler number Da≤1) and their size evolution was monitored with the dynamic and static light scattering methods (DLS and SLS). The size of primary nanoparticles (nuclei) $2R_0$=3.6 nm was confirmed by DLS and TEM experiments and found to be almost independent on the reaction conditions.

A remarkable similarity with the titanium-oxo-alkoxy (TOA) nanoparticles was observed. In particularly, both ZOA and TOA systems show quasi-instantaneous nucleation and "classical" accelerated particles growth on the induction stage for hydrolysis ratios H>2.0 and stable colloids for H≤2.0. High reaction orders (>1) of metal-oxo-alkoxy species is confirmed in agreement with the model, which assumes partial irreversibility of the hydrolysis-condensation reactions. Both ZOA and TOA sol nanoparticles grow as low-dimension 1D fractals during the induction stage. However in contrast to TOA, ZOA species show up no stable hierarchical units (clusters) with $R_0 \geq R \geq 1$ nm, which makes these colloids less stable against aggregation that increases polydispersity of sol nanoparticles. The observed features can be inherent to hierarchical metal-oxo-alkoxy species formation in the sol-gel process. More experiments and theoretical support are required to elucidate stable sub-nucleus ZOA units and critical hydrolysis ratio permitted nucleation.

Acknowledgments. ANR (Agence Nationale de la Recherche) and CGI (Commissariat à l'Investissement d'Avenir) are gratefully acknowledged for their financial support of this work through Labex SEAM (Science and Engineering for Advanced Materials and devices) ANR 11 LABX 086, ANR 11 IDEX 05 02.

References

1. C. J. Brinker, G. W. Scherer, *Sol-Gel Science: The Physics and Chemistry of Sol-Gel Processing*, Academic Press, New-York, 1990.
2. Pierre, A. C. *Introduction to Sol-Gel Processing*, Kluwer Int. Ser. in Sol-Gel Processing: Technology and Applications, Kluwer, 1998.
3. G. A. Seisenbaeva and Vadim G. Kessler, *Nanoscale*, 2014, **6**, 6229.
4. M. Yoshimura, *J. Mater. Sci.*, 2006, **41**, 1299.
5. T. Sasaki, Y. Mori, F. Kawamura, M. Yoshimura and Y. Kitaoka, *J. Cryst. Growth*, 2008, **310**, 1288.
6. V. G. Kessler, *J. Sol-Gel Sci. Technol.*, 2009, **51**, 264.
7. G. A. Seisenbaeva, V. G. Kessler, R. Pazik and W. Strek, *Dalton Trans.*, 2008, **3412**.
8. L. Rozes, N. Steunou, G. Fornasieri and C. Sanchez, *Monatshefte für Chemie*, 2006, **137**, 501.
9. R. Azouani, A. Soloviev, M. Benmami, K. Chhor, J-F. Bocquet and A. Kanaev *J. Phys. Chem. C*, 2007, **111**, 16243.
10. A. Clearfield, *J. Materials Research*, 1990, **5**, 161.
11. W. J. Evans M. A. Ansari and J. W. Ziller, *Polyhedron*, 1998, **17**, 869.
12. G. I. Spijksma, G. A. Seisenbaeva, A. Fischer, H. J. M. Bouwmeester, D. H. A. Blank and V. G. Kessler, J Sol-Gel Sci Technol, 2009, **51**, 10.
13. G. I. Spijksma, G. A. Seisenbaeva, H. J. M. Bouwmeester, D. H. A. Blank and V. G. Kessler, *Polyhedron*, 2013, **53**, 150.
14. G. Ehrhart, B. Capoen, O. Robbe, Ph. Boy, S. Turrell and M. Bouazaoui, *Thin Solid Films*, 2006, **496**, 227.
15. M. T. Soo, N. Prastomo, A. Matsuda, G. Kawamura, H. Muto, A. F. M. Noor, Z. Lockman and K. Y. Cheong, *Appl. Surf. Sci.*, 2012, **258**, 5250.

16. C.-F. Chang, C.-Y. Chang and T.-L. Hsu, *Colloids and Surfaces A*, 2008, **327**, 64.

17. J. C. S. Wu and L. C. Cheng, *J. Membrane Sci.*, 2000, **167**, 253.

18. W. Huang, J. Yang, X. Meng, Y. Cheng, C. Wang, B. Zou, Z. Khan, Z. Wang and X.Cao, *Chem. Eng. J.*, 2011, **168**, 1360.

19. J. A. Wang, M. A. Valenzuela, J. Salmones, A. Vázquez, A. García-Ruiz and X. Bokhimi, *Catal. Today*, 2001, **68**, 21.

20. F. Davar, A. Hassankhani and M. R. Loghman-Estarki, *Ceramics Int.*, 2013, **39**, 2933.

21. M. C. Silva, G. Trolliard, O. Masson, R. Guinebretiere, A. Dauger, A. Lecomte and B. Frit, *J. Sol-Gel Sci. Technol.*, 1997, **8**, 419.

22. D. A. Zyuzin, E. M. Moroz, A. S. Ivanova and A. N. Shmakov, *Crystallography Reports*, 2003, **48**, 413.

23. D. A. Zyuzin, E. M. Moroz, A. S. Ivanova, A. N. Shmakov and G. N. Kustova, *Kinetics and Catalysis*, 2004, **45**, 739.

24. V. K. Ivanov, G. P. Kopitsa, O. S. Ivanova, A. Ye. Baranchikov, K. Pranzas and S. V. Grigoriev, *J. Phys. Chem. of Solids*, 2014, **75**, 296.

25. A. I. Kuznetsov, O. Kameneva, N. Bityurin, L. Rozes, C. Sanchez and A. Kanaev, *Phys. Chem. Chem. Phys.*, 2009, **11**, 1248.

26. P. Gorbovyi, A. Uklein, S. Tieng, M. Traore, K. Chhor, L. Museur and A. Kanaev, *Nanoscale*, 2011, **3**, 1807.

27. C. Piconi and G. Maccauro, *Biomaterials*, 1999, **20**, 1.

28. E. De la Rosa-Cruz, L. A. Diaz-Torres, P. Salas, V. M. Castano and J. M. Hernandez, *J Phys. D*, 2001, **34**, L83.

29. M. Shane and M. L. Mecartney, *J. Mater. Sci.*, 1990, **25**, 1537.

30. T. Yamaguchi, *Catal. Today*, 1994, **20**, 199.

31. R. L. Z. Hoye, K. P. Musselman and J. L. MacManus-Driscoll, *Apl. Materials*, 2013, **1**, 060701.

32. J. Bałdyga and R. Pohorecki, *Chem. Eng. J.*, 1995, **58**, 183.

33. M. Rivallin, M. Benmami, A. Kanaev and A. Gaunand, *Chem. Eng. Res. Design*, 2005, **83**, 67.

34. R. Azouani, A. Michau, K. Hassouni, K. Chhor, J.-F. Bocquet, J.-L. Vignes and A. Kanaev, *Chem. Eng. Res. Design*, 2010, **88**, 1123.

35. J. Livage, M. Henry and C. Sanchez, *Prog. Solid-State Chem.*, 1988, **18**, 259.

36. M. Bouslama, M. C. Amamra, Z. Jia, M. Ben Amar, O. Brinza, K. Chhor, M. Abderrabba**,** J.-L. Vignes and A. Kanaev, *ASC Catal.*, 2012, **2**, 1884.

37. O. Khatim, M. Amamra, K. Chhor, T. Bell, D. Novikov, D. Vrel and A. Kanaev, *Chem. Phys. Lett.*, 2013, **558**, 53.

38. M. Rivallin, M. Benmami, A. Gaunand and A. Kanaev, *Chem. Phys. Lett.*, 2005, **398**, 157.

39. V. K. LaMer and R. H. Dinegar, *J. Am. Chem. Soc*., 1950, **72**, 418.

40. J. S. Chappel, L. J. Procopio and J. D. Birchall, *J. Mat. Sci. Letters*, 1990, **9**, 1329

41. K. Dehnicke, J. Weidlein, *Angew. Chem. Int. Edit.*, 1966, **5**, 1041.

42. C. J. Hardy, B. O. Field, D. Scargillj, *J. Inorg. Nucl. Chem.*, 1966, **28**, 2408.

43. R. Sathiyanarayanan, M. Alimohammadi, Y. Zhou and K. A. Fichthorn, *J. Phys. Chem. C*, 2011, **115**, 18983.

44. F. Wang, V. N. Richards, S. P. Shields and W. E. Buhro, *Chem. Mater.*, 2014, **26**, 5.

45. A. Soloviev, H. Jensen, E. G. Søgaard and A. V. Kanaev, *J. Mater. Sci.*, 2003, **38**, 3315.

Tables

Table 1. Initial radius of the ZOA particles (R_0) and induction time (t_{ind}) of the sol-gel process using ZNP precursor in-propanol (C_{Zr}=0.15 mol/l, T=20 °C) for different hydrolysis ratios H.

$H = C_{H2O}/C_{Zr}$	R_0, nm (±0.1 nm)	t_{ind}, s
1.0	1.55	Inf
1.2	1.65	Inf
1.5	1.65	Inf
1.7	1.80	Inf
2.0	1.80	Inf
2.1	1.80	$7.48 \cdot 10^4$
2.2	1.85	$2.14 \cdot 10^4$
2.3	1.95	5690
2.4	1.80	2960
2.5	1.95	1900
2.6	2.15	1410
2.7	-	618

Table 2. Initial radius of the ZOA particles (R_0) and induction time (t_{ind}) of the sol-gel process in-propanol (H=2.5, T=20 °C) for different ZNP concentrations (C_{Zr}).

C_{Zr}, mol/l	R_0, nm (±0.1 nm)	t_{ind}, s
0.100	2.1	80890
0.120	2.2	7870
0.130	2.0	4200
0.140	1.9	2010
0.150	1.9	1910

Table 3. Model parameters *a* and *b* of Equation (3) obtained from experiment.

Series	Parameter	h^*	
		h^*=2.0	h^*=1.5
H variable	b	2.4	6.6
C_{Zr} variable	a+b	6.3	
Results	b	2.4	6.6
	a	3.9	-0.3

Figure captions

Figure 1. Characteristic ACFs of ZOA nanoparticles in the beginning of the sol-gel growth using different precursor/solvent pairs: ZNB in n-butanol (a), ZNB in 2-propanol (b), ZNB in ethanol (c) and ZNP in n-propanol (d) (C_{Zr}=0.15 mol/l, H>2, T=20 °C).

Figure 2. ACFs of ZOA nanoparticles in ZNP/n-propanol solution at low hydrolysis ratios: H=1.0 (a), 1.5 (b) and 1.8 (c) (C_{Zr}=0.15 mol/l, T=20 °C).

Figure 3. Temporal evolution of the scattered light intensity (I) and oarticle size (R) during induction period of the ZNP/n-propanol sol-gel process for different hydrolysis ration H≥2.0 (C_{Zr}=0.15 mol/l, T=20 °C).

Figure 4. Temporal evolution of the scattered light intensity during induction period of the ZNP/n-propanol sol-gel process for zirconia concentrations C_{Zr}=0.10 (a), 0.12 (b), 0.13 (c) and 0.15 (d) mol/l (H=2.5, T=20 °C) (H=2.5, T=20 °C).

Figure 5. Slope of I(t) curves versus induction rate ($1/t_{ind}$) during the induction period of the ZNP/n-propanol sol-gel process for different hydrolysis ration H≥2.0 (C_{Zr}=0.15 mol/l, T=20 °C). Linear fir is given by the solid line.

Figure 6. Initial particles size (R_0) and slope of I(t) curves during the induction period of the ZNP/n-propanol sol-gel process for different hydrolysis ration H≥2.0 (C_{Zr}=0.15 mol/l, T=20 °C).

Figure 7. MET image of the ZOA nanoparticles (C_{Zr}=0.15 mol/l, H=2.5, T=20 °C).

Figure 8. Dependence of the induction rate on zirconium concentration (H=2.5, T=20 °C).

Figure 9. Dependence of the induction rate on the hydrolysis ratio excess above critical value h^*=1.5 (a) and 2.0 (b) (C_{Zr}=0.15 mol/l, T=20 °C).

Fig. 1

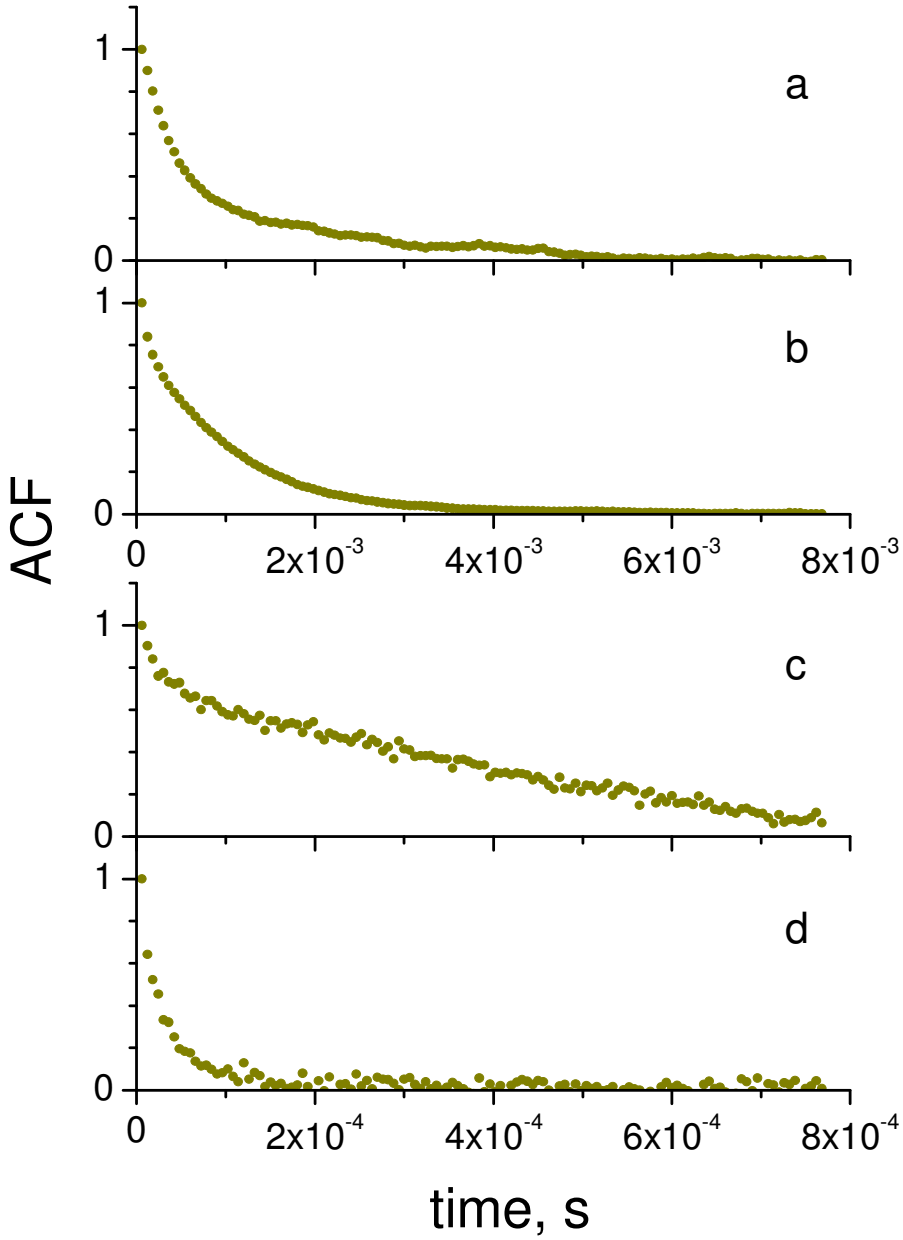

Fig. 2

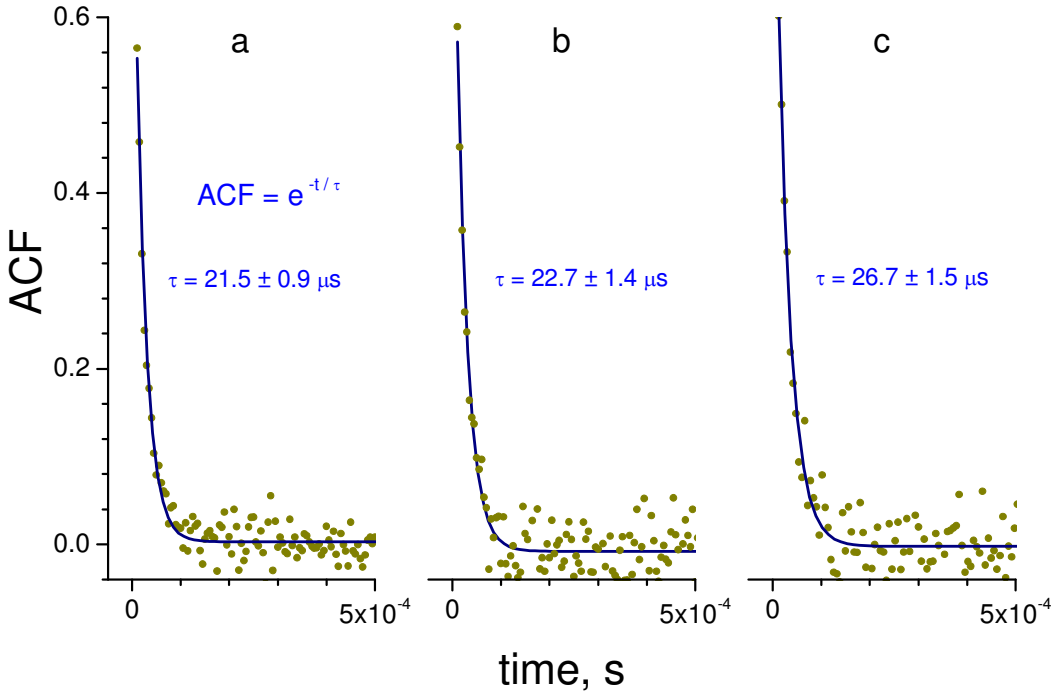

Fig. 3

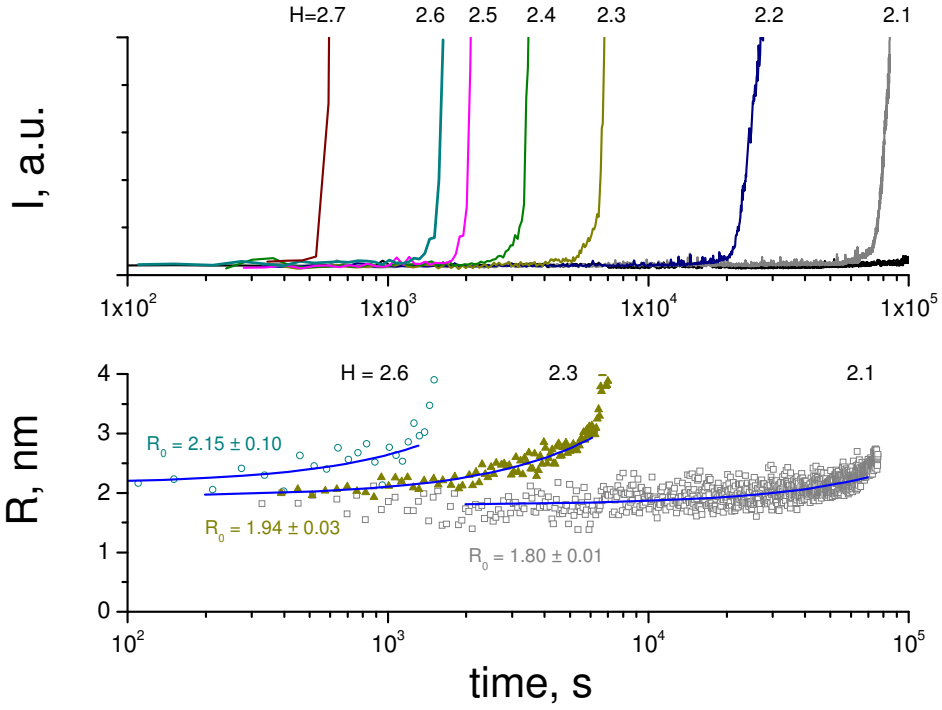

Fig. 4

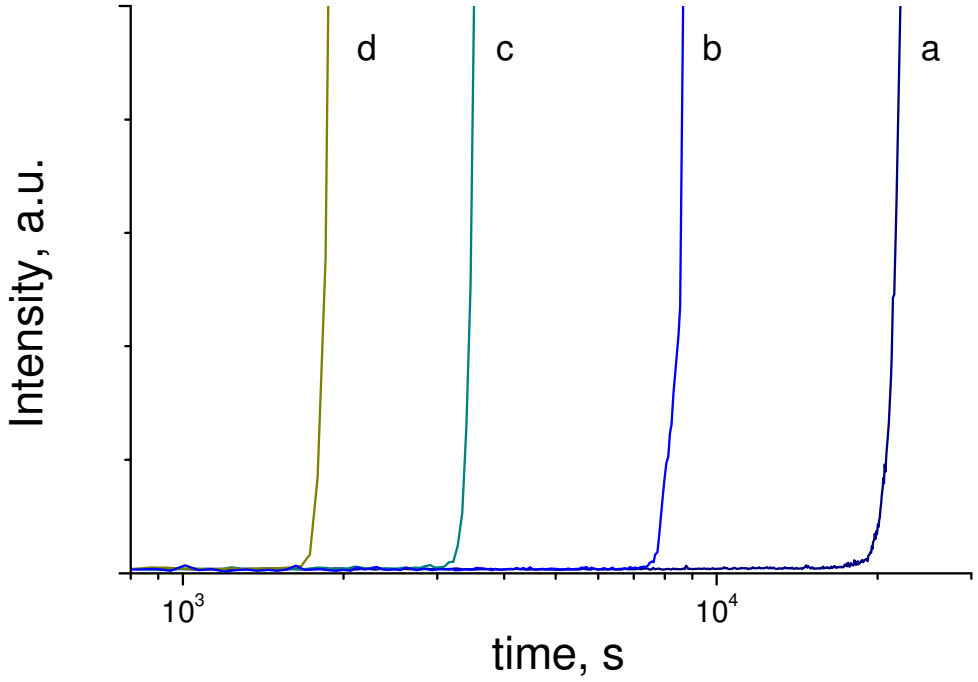

Fig. 5

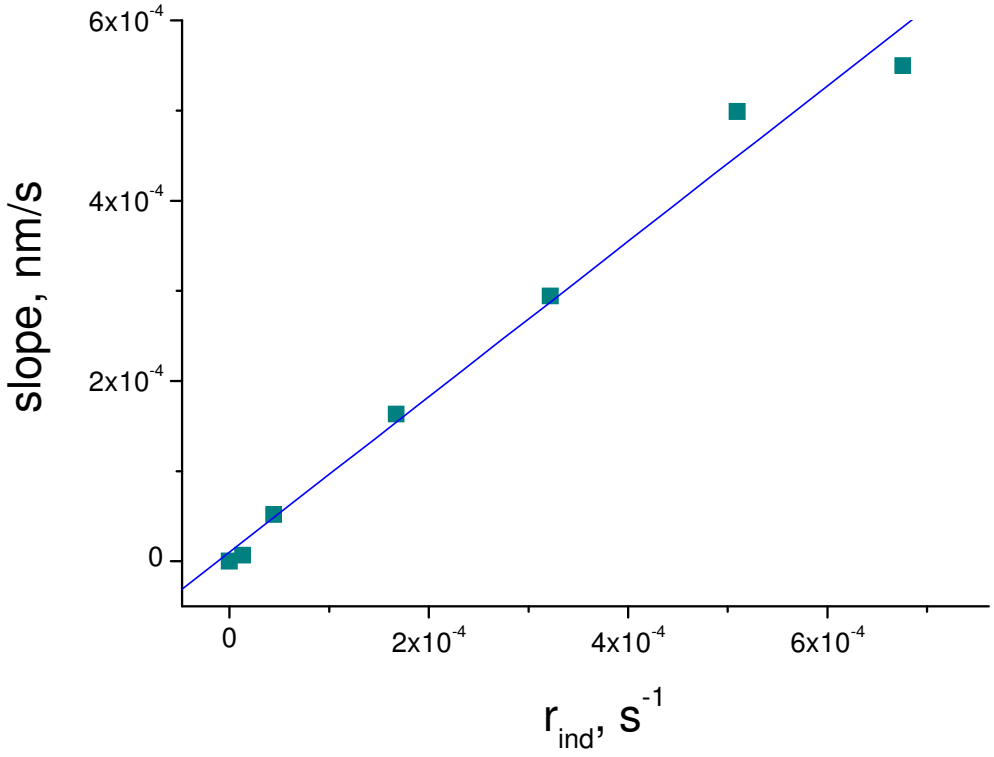

Fig. 6

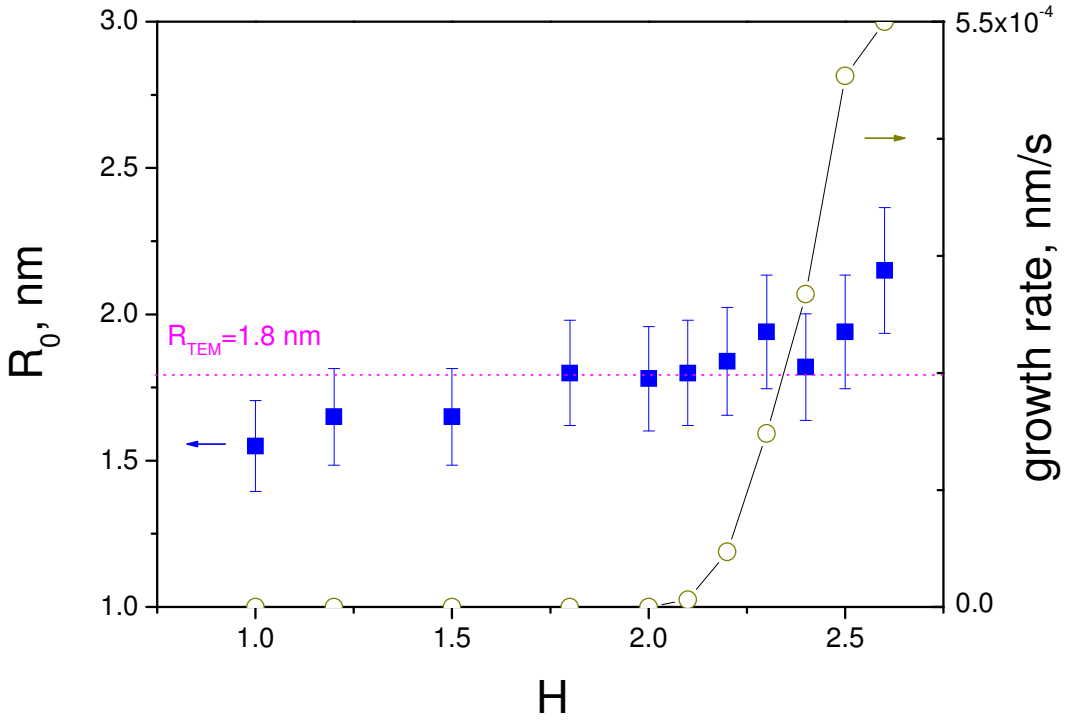

Fig. 7

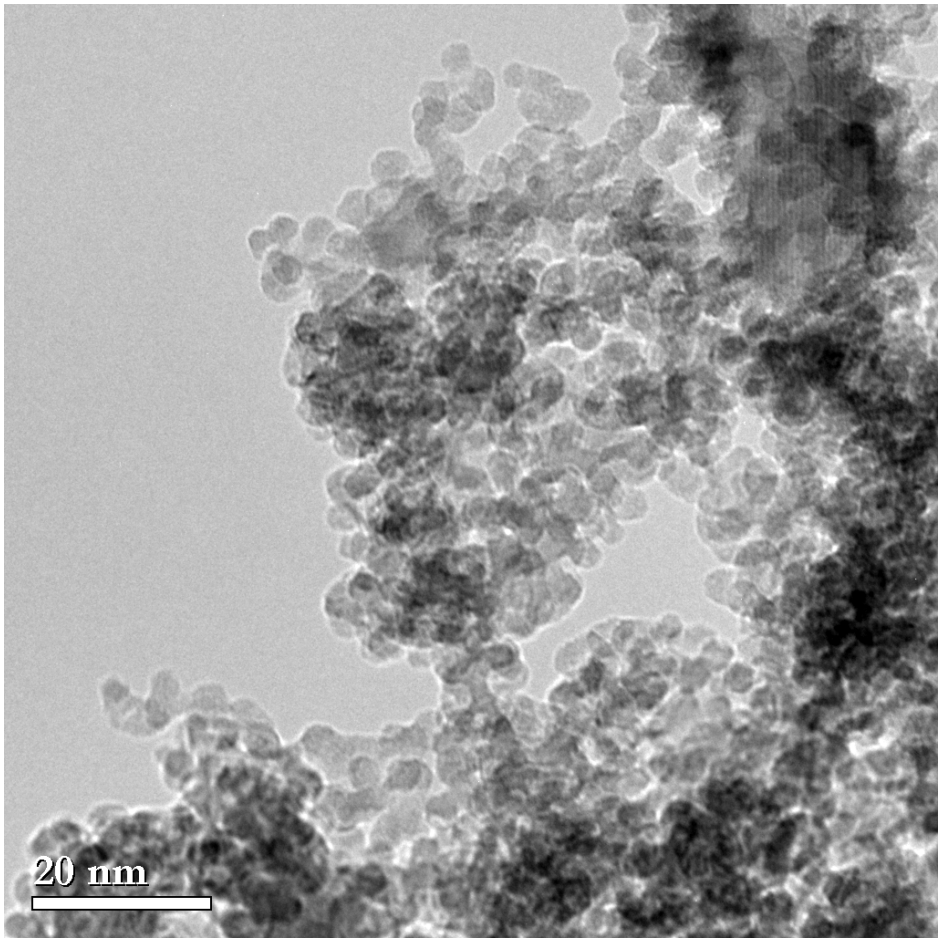

Fig. 8

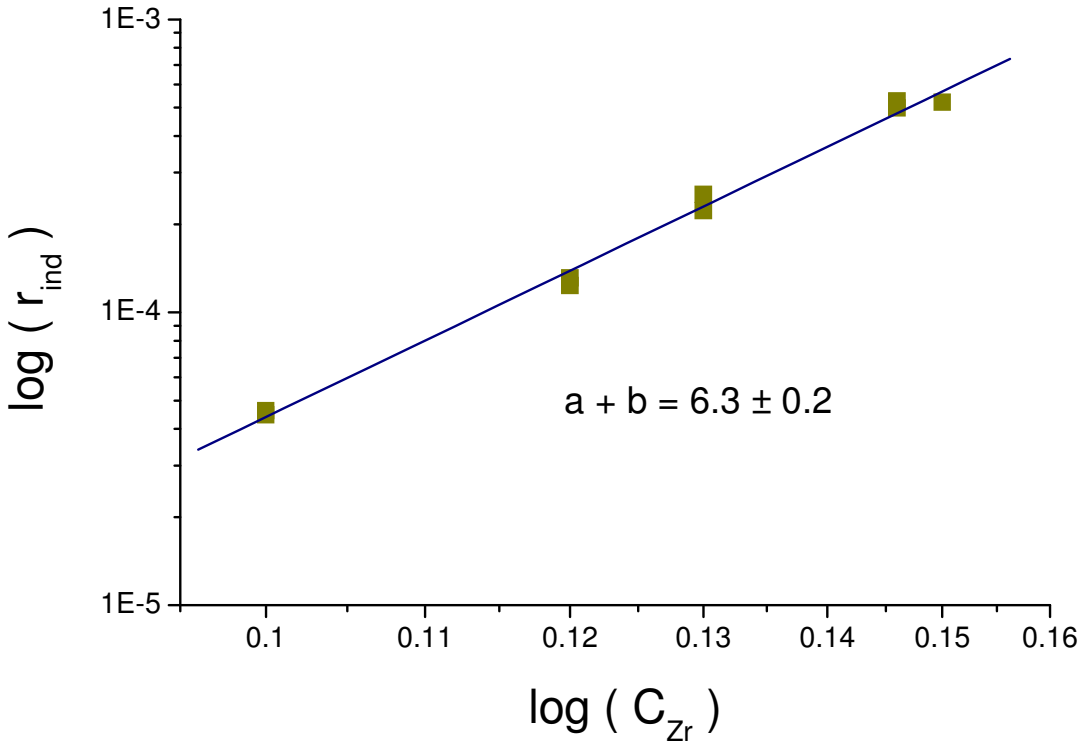

Fig. 9